ISBN: 978-3-95450-232-5 ISSN: 2673-7000 doi:10.18429/JACoW-NAPAC2022-MOPA57

ONLINE MODELS FOR X-RAY BEAMLINES*

Boaz Nash, Dan T. Abell, Michael Keilman,
Paul Moeller, Ilya V. Pogorelov, RadiaSoft LLC, Boulder, CO, USA
Yonghua Du, Abigail Giles, Joshua Lynch, Thomas Morris,
Maksim Rakitin, Andrew L. Walter, BNL, Upton, NY, USA
Nicholas Goldring, STATE33 INC, Portland, OR, USA

Abstract

X-ray beamlines transport synchrotron radiation from the magnetic source to the sample at a synchrotron light source. Alignment of elements such as mirrors and gratings are often done manually and can be quite time consuming. The use of photon beam models during operations is not common in the same way that they are used to great benefit for particle beams in accelerators. Linear and non-linear optics including the effects of coherence may be computed from source properties and augmented with measurements. In collaboration with NSLS-II, we are developing software tools and methods to include the model of the x-ray beam as it passes on its way to the sample. We are integrating the Blue-Sky beamline control toolkit with the Sirepo interface to several x-ray optics codes. Further, we are developing a simplified linear optics approach based on a Gauss-Schell model and linear canonical transforms as well as developing Machine Learning models for use directly from diagnostics data. We present progress on applying these ideas on NSLS-II beamlines and give a future outlook on this rather large and open domain for technological development.

INTRODUCTION

Here we present further progress in the development of reduced models for use during real-time operation of X-ray beamlines. In Ref. [1], we introduced the concept of a matrix-aperture beamline composed of linear transport sections and physical apertures as shown in Fig. 1. This approach is an approximation with the hope of capturing important transport properties in a computationally efficient manner. Within this approach there exists a hierarchy of methods[1] as shown in Fig. 2. The first row of the table involves second moment propagation representing Gaussian Wigner functions [3]. The second row of the table involves propagating coherent electric fields via linear canonical transform (LCT). Progress in creation of an LCT transport library is reported in Ref. [4]. The final row of the table represents generic partially coherent X-ray propagation via Wigner function passing through the matrix-aperture beamline. Some work towards developing this method was presented in Ref. [5]. The focus of this paper will be the top level method of sigma matrix transport through the matrix-aperture beamline. We refer to this reduced model as the Gaussian Wigner function moment (GWFM) model. This model provides a computationally efficient calculation of the linear optics through the beamline while also including effects of partial coherence. We apply the sigma matrix transport method to a KB mirror beamline with two apertures and compare results with SRW and Shadow. Finally, the realistic case of an NSLS-II beamline is treated with this method and preliminary results are presented.

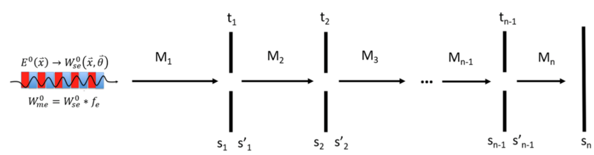

Figure 1: Matrix-aperture beamline schematic with n linear transport sections and $n-1$ apertures. M_j represents the transport matrix across the j^{th} section of the beamline (from position s_{j-1} to s_j) and t_j represents the transfer function of the j^{th} aperture. An undulator source is depicted in this figure creating partially coherent synchrotron radiation.

$\vec{z}_i$	M_1	t_1		M_2	t_2		M_3	$\vec{z}_f$
Σ_i	$\mathcal{S}_{M_1}$	Σ_1	Σ_1'	$\mathcal{S}_{M_2}$	Σ_2	Σ_2'	$\mathcal{S}_{M_3}$	Σ_f
$\vec{E}_i$	$\mathcal{L}_{M_1}$	$\vec{E}_1$	$\vec{E}_1'$	$\mathcal{L}_{M_2}$	$\vec{E}_2$	$\vec{E}_2'$	$\mathcal{L}_{M_3}$	$\vec{E}_f$
W_i	$\mathcal{T}_{M_1}$	W_1	W_1'	$\mathcal{T}_{M_2}$	W_2	W_2'	$\mathcal{T}_{M_3}$	W_f

Figure 2: Hierarchy of reduced models for radiation transport through a matrix-aperture beamline.

We remind the reader that the goal of such fast reduced models is to enable the creation of online models incorporating up-to-the-moment diagnostics data such that the model accurately reflects the true state of the beamline settings and X-ray transport from source to sample. Such an online model may be used to automate precise tuning and alignment of the beamline. In addition to physics-based models, we are also developing machine learning-based models for the same purpose. See Ref. [6] for further information on the progress of this effort.

KB MIRROR BEAMLINE

We consider the case of a KB mirror beamline with successive horizontally and vertically focusing mirrors as shown in Fig. 3. We have setup this beamline within the Shadow code to illustrate the method of moment propagation through a matrix-aperture beamline. The transfer matrices along the

* Work supported by the US Department of Energy, Office of Basic Energy Sciences under Award No. DE-SC0020593.

[1] We do not intend to be comprehensive in our scope of all work pertaining to reduced models here. The hybrid method [2] may fit closely within our schema as an alternative to the LCT method, combining wavefront propagation with ray tracing.

Content from this work may be used under the terms of the CC BY 4.0 licence (© 2022). Any distribution of this work must maintain attribution to the author(s), title of the work, publisher, and DOI

ISBN: 978-3-95450-232-5 ISSN: 2673-7000 doi:10.18429/JACoW-NAPAC2022-MOPA57

beamline are computed as described in Ref. [1]. In addition, we introduce a rectangular aperture 14 meters from the source. The horizontal and vertical sizes of an aperture in Shadow are represented by the variables RX_SLIT and RY_SLIT respectively and correspond to $2a_h$ within our analysis [3]. As discussed therein, the Gaussian aperture size, a_g, is proportional to the hard-edge aperture size, a_h, with the proportionality factor weakly dependent on beam parameters (details are currently under study). For this work, we assumed $a_g = a_h$.

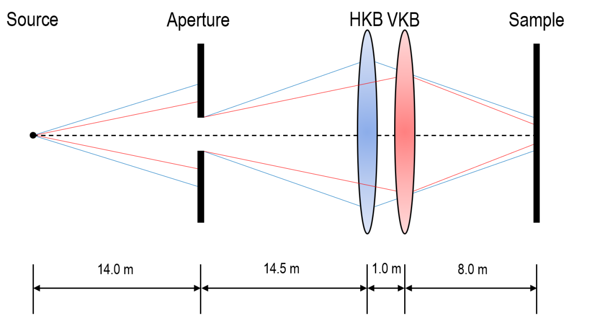

Figure 3: Diagram of KB-mirror beamline with beam defining aperture. Blue and red lines represent horizontal and vertical beam projection respectively. HKB and VKB are horizontally and vertically focusing elliptical mirrors represented by lenses in the diagram.

For this study, we define an initial beam size of 45 µm in the horizontal and 25 µm in the vertical and consider a wavelength, λ, of 1.24 nm corresponding to an energy of 1 keV. We define the divergences according to the following equation:

$$\sigma_{x,y}\sigma_{\theta_{x,y}} = m^2_{x,y}\frac{\lambda}{4\pi} \tag{1}$$

where $m^2_{x,y}$ is known as the beam quality factor in the optics literature. $m_{x,y} = 1$ represents the coherent case and $m_{x,y} > 1$ represents the partially coherent case. For the coherent case, the divergences are $\sigma_{\theta_x} = 2.2$ µrad and $\sigma_{\theta_y} = 3.9$ µrad. In the partially coherent case, the divergences will be larger.

We propagate this beam in the highly but not fully coherent case of $m^2_x = m^2_y = 1.1$. Figure 4 shows the beam size propagation through the KB-mirror beamline in the nominal case without apertures. The beam size evolution with rectangular hard-edge aperture of size $a_{h_x} = 50$ µm and $a_{h_y} = 45$ µm is shown in Fig. 5.

Next we consider the evolution of the photon beam emittance which is defined analogously to the quantity in beam dynamics as

$$\epsilon = \sqrt{\sigma_{xx}\sigma_{\theta_x\theta_x} - \sigma^2_{x\theta_x}}\,. \tag{2}$$

The evolution of the emittance down the KB aperture beamline is shown in Fig. 6 for increasing value of beam quality factor. We first note that linear sections preserve the emittance. In the coherent case, the emittance is also conserved across the aperture. However, as the coherence decreases, one finds that the emittance decreases more and more across the aperture.

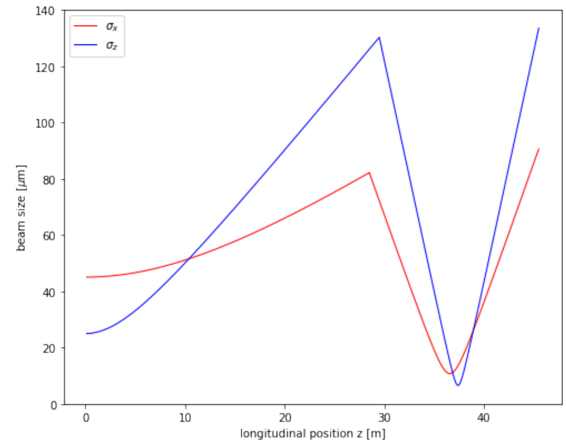

Figure 4: Horizontal and vertical X-ray beam size evolution through KB beamline without aperture. The ray-tracing code Shadow was used for the transfer matrix calculations.

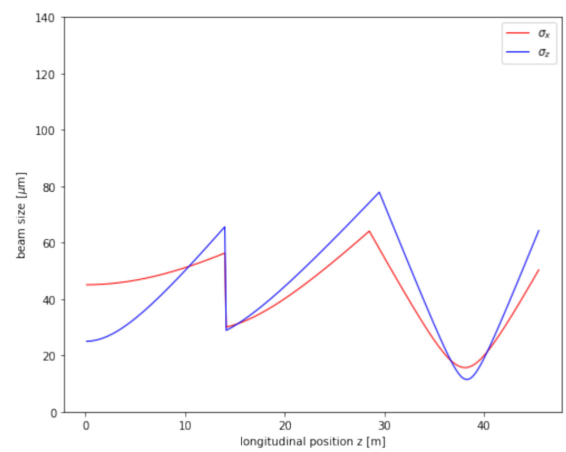

Figure 5: Horizontal and vertical X-ray beam size evolution through KB beamline with Gaussian aperture.

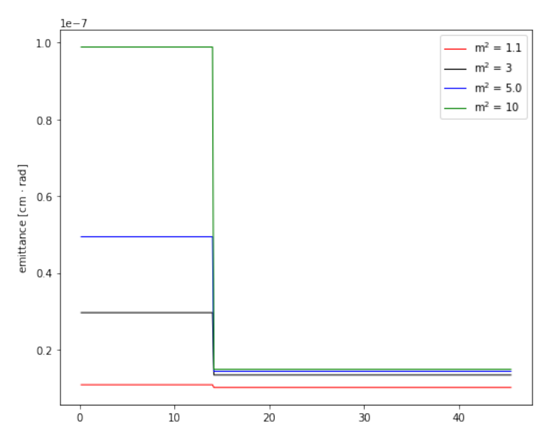

Figure 6: Evolution of horizontal X-ray beam emittance through KB-mirror aperture beamline with varying values of beam quality factor.

Content from this work may be used under the terms of the CC BY 4.0 licence (© 2022). Any distribution of this work must maintain attribution to the author(s), title of the work, publisher, and DOI

ISBN: 978-3-95450-232-5 ISSN: 2673-7000 doi:10.18429/JACoW-NAPAC2022-MOPA57

Content from this work may be used under the terms of the CC BY 4.0 licence (© 2022). Any distribution of this work must maintain attribution to the author(s), title of the work, publisher, and DOI

A remarkable feature of our GWFM model is that coherence length may be calculated from the second moment matrix, Σ. Using Eq. (1) and the results in Ref. [3], the expression for coherence length may be written as[2]

$$\xi = \frac{2\sigma_x}{\sqrt{m^4 - 1}} \, . \tag{3}$$

The coherence length evolution for the KB aperture beamline is plotted in Fig. 7 for increasing value of beam quality factor. We recall the interesting result of Ref. [3] that the coherence length does not change when passing through the Gaussian aperture which can be seen when examining the aperture position (14 meters) in Fig. 7.

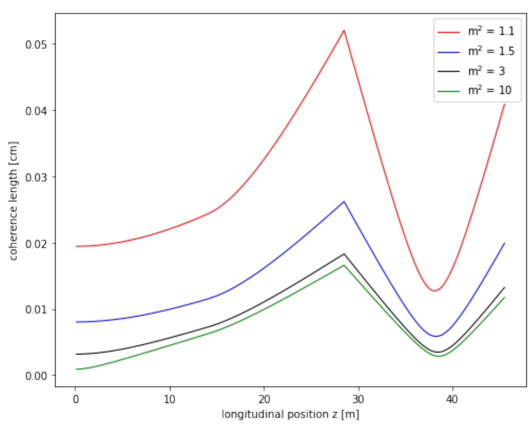

Figure 7: Evolution of horizontal coherence length through KB-mirror aperture beamline with varying values of beam quality factor.

We note that the beam size clearly decreases when passing through the aperture but the coherence length does not. This implies that the beam quality factor must also decrease in accordance with Eq. (3). More generally, there is another representation of coherence referred to as the degree of coherence, μ. This quantity is defined in terms of the Wigner function as [8]:

$$\mu^2 = \lambda^2 \int W^2(\vec{z}) d\vec{z} \tag{4}$$

where $\vec{z}$ is the 4D phase space vector.

In the case of a Gaussian Wigner function, the degree of coherence works out to be

$$\mu = \frac{\lambda}{4\pi (\det \Sigma)^{1/4}} \tag{5}$$

which reduces to

$$\mu = \frac{1}{m_x m_y} \tag{6}$$

in the absence of x-y coupling.

[2] A general expression for coherence length in the 4D case can be found in Ref. [7].

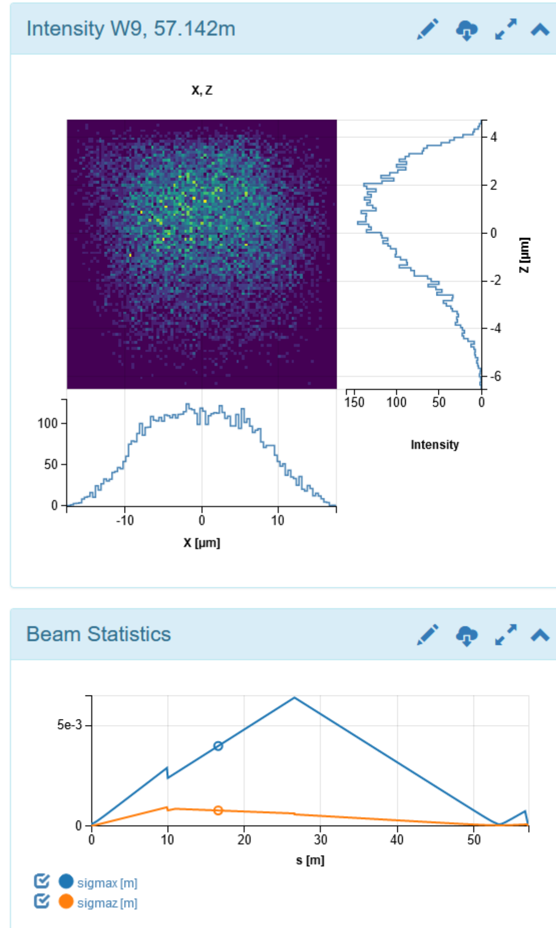

Figure 8: Final intensity plot and beam statistics report in Sirepo-Shadow interface for NSLS-II TES beamline.

CONCLUSION AND OUTLOOK

We summarize some reduced models for X-ray beamlines focusing on our recent results for a GWFM model. These formulae have been integrated into the Shadow ray tracing code allowing for propagation of moments through realistic beamlines including focusing elements and physical apertures. For a simple KB aperture beamline, we demonstrated this method showing how beam size, emittance, and coherence length evolve down the beamline. We are in the process of integrating the GWFM model into the Sirepo-Shadow interface. A screenshot of this integration is shown in Fig. 8 where the NSLS-II TES beamline has been modeled both with Shadow-Sirepo and the GWFM model (beam statistics report).

A future goal involves integrating this model within an X-ray beamline control system. The Bluesky software used for beamline control has been integrated into the Sirepo suite of beamline modeling tools via the software package Sirepo-Bluesky [9, 10]. Recent developments enable access to Shadow-based computations and thus our reduced models become available for use in beamline control algorithms.

ISBN: 978-3-95450-232-5 ISSN: 2673-7000 doi:10.18429/JACoW-NAPAC2022-MOPA57

REFERENCES

[1] B. Nash, N. Goldring, J. Edelen, C. Federer, P. Moeller, and S. Webb, "Reduced model representation of x-ray transport suitable for beamline control," in *Proc. Advances in Computational Methods for X-Ray Optics V*, International Society for Optics and Photonics, vol. 11493, 2020, pp. 53–61. doi:10.1117/12.2568187

[2] X. Shi, R. Reininger, M. Sanchez del Rio, and L. Assoufid, "A hybrid method for X-ray optics simulation: combining geometric ray-tracing and wavefront propagation," *J. Synchrotron Radiat.*, vol. 21, no. 4, pp. 669–678, 2014. doi: 10.1107/S160057751400650X

[3] B. Nash, D. Abell, N. Goldring, P. Moeller, and I. Pogorelov, "Propagation of Gaussian Wigner Function Through a Matrix-Aperture Beamline," in *Proc. IPAC'22*, Bangkok, Thailand, 2022, paper THPOPT067, pp. 2755–2758. doi:10.18429/JACoW-IPAC2022-THPOPT067

[4] B. Nash, D. Abell, N. Goldring, P. Moeller, and I. Pogorelov, "Linear Canonical Transform Library for Fast Coherent X-Ray Wavefront Propagation," in *Proc. IPAC'22*, Bangkok, Thailand, 2022, paper THPOPT068, pp. 2759–2762. doi: 10.18429/JACoW-IPAC2022-THPOPT068

[5] B. Nash, N. Goldring, J. Edelen, S. Webb, and R. Celestre, "Propagation of partially coherent radiation using Wigner functions," *Phys. Rev. Accel. Beams*, vol. 24, no. 1, p. 010 702, 2021. doi:10.1103/PhysRevAccelBeams.24.010702

[6] T. Morris *et al.*, "On-the-fly optimization of synchrotron beamlines using machine learning," in *Optical System Alignment, Tolerancing, and Verification XIV*, 2022.

[7] R. Simon, E. C. G. Sudarshan, and N. Mukunda, "Anisotropic Gaussian Schell-model beams: Passage through optical systems and associated invariants," *Phys. Rev. A*, vol. 31, no. 4, pp. 2419–2434, 1985. doi:10.1103/PhysRevA.31.2419

[8] I. V. Bazarov, "Synchrotron radiation representation in phase space," *Phys. Rev. Spec. Top. Accel. Beams*, vol. 15, no. 5, p. 050 703, 2012. doi:10.1103/PhysRevSTAB.15. 050703

[9] Nsls-II, *sirepo-bluesky*, https://github.com/NSLS-II/sirepo-bluesky

[10] M. S. Rakitin *et al.*, "Introduction of the Sirepo-Bluesky interface and its application to the optimization problems," in *Proc. Advances in Computational Methods for X-Ray Optics V*, International Society for Optics and Photonics, vol. 11493, 2020, pp. 209–226. doi:10.1117/12.2569000

Content from this work may be used under the terms of the CC BY 4.0 licence (© 2022). Any distribution of this work must maintain attribution to the author(s), title of the work, publisher, and DOI